Preprint Title	Effect of Different Silica Coatings on the Toxicity of upconversion nanoparticles on RAW 264.7 macrophage cells
Authors	Cynthia E. Kembuan, Helena Oliveira and Christina Graf
Publication Date	04 Sep 2020
Article Type	Full Research Paper
Supporting Information File 1	Supporting Information Kembuan et al_2020_Cytotoxicity_Silica_UCNP.pdf; 174.6 KB
ORCID® iDs	Helena Oliveira - https://orcid.org/0000-0002-4673-0696; Christina Graf - https://orcid.org/0000-0002-3308-5640

Effect of Different Silica Coatings on the Toxicity of upconversion nanoparticles on RAW 264.7 macrophage cells

Cynthia Kembuan,[1] Helena Oliveira,[2] and Christina Graf*[3]

Address: [1]Institut für Chemie und Biochemie, Physikalische und Theoretische Chemie, Freie Universität Berlin, Takustraße 3, D-14195 Berlin, Germany, [2], Department of Biology & CESAM, University of Aveiro, 3810-193 Aveiro, Portugal, and [3]Hochschule Darmstadt - University of Applied Sciences, Fachbereich Chemie- und Biotechnologie, Stephanstr. 7, D-64295 Darmstadt, Germany

Email: Christina Graf - christina.graf@h-da.de
* Corresponding author

Abstract

Upconversion nanoparticles (UCNP) consisting of $NaYF_4$ doped with 18% Yb and 2% Er were coated with microporous silica shells of 7±2 nm and 21±3 nm thickness. Subsequently, the initially negatively charged particles were optionally functionalized with N-(6-aminohexyl)-aminopropyltrimethoxysilane (AHAPS), providing a positive charge onto the nanoparticle surface. Inductively coupled plasma optical emission spectrometry (ICP-OES) measurements revealed that the particles with the thicker shells release fewer lanthanide ions in 24 h than particles with a thinner shell but that even a 21±3 nm thick silica layer does not entirely block the disintegration process of

the UCNP. MTT tests and cell cytometry measurements with macrophages (RAW 264.7 cells) indicate that the cells treated with amino-functionalized particles with a thicker silica shell have higher viability than those incubated with UCNP with a thinner silica shell even if more particles with a thicker shell are taken up. This effect is less significant for negatively charged particles. A cell cycle analysis with amino-functionalized particles also confirms that a thicker silica shell reduces the cytotoxicity. Thus, growing silica shells of sufficient thickness is a simple approach to minimize the cytotoxicity of UCNP.

Keywords

upconversion nanoparticles; silica coating; cytotoxicity; RAW 264.7 macrophage cells; ion release

Introduction

Upconversion nanoparticles (UCNP) convert excitation radiation with long wavelengths to short-wavelength emission. Since biological molecules do not show upconversion, imaging with UCNP avoids autofluorescence. Besides, UCNP have further advantages for applications in life science such as deep penetration depth, minimal photodamage, and high resistance to photobleaching. [1-9] Moreover, high thermal and photochemical stability, as well as high chemical inertness and relatively low toxicity, also are claimed. [7, 10, 11] Due to these unique features, UCNP have already been used in medical and biological applications such as multimodal bioimaging, drug delivery, photodynamic therapy, and biosensing. [12-17]

However, UCNP in aqueous dispersions undergo to some extent of disintegration, which also results in the quenching of their luminescence intensity. [8, 10, 18-24] This

concentration-dependent effect is especially significant when the dispersions are highly diluted, [8, 19, 23] the pH is low, [23] or ions forming lanthanide salts with low solubility such as phosphate are present, [10, 20, 25] which is relevant for their application in physiological solutions. The cytotoxicity of F^- is in the range of a few mM. [26, 27] The release of F^- can induce oxidative stress and cause apoptosis and also, intracellular redox homeostasis and gene expression can be modulated. [27] Lanthanide ions are usually not reported as highly toxic; however, they can interact with proteins, enzymes, and other biomolecules [28, 29] and might also cause oxidative damage or lipid peroxidation. [30]

If UCNP are applied in life science, it is usually necessary to modify their surfaces with hydrophilic ligands or layers. [22, 31, 32] Such coatings can also prevent, to some extent, the interaction of the UCNP with the aqueous environment and consequently reduce their disintegration processes in an aqueous environment. Several authors have reported the use of protective coatings such as poly(acrylic acid) and poly(allylamine hydrochloride), [18] multichelating phosphonate, [31, 33, 34] block copolymers, [35] amphiphilic polymers, [8, 22], or polysulfonates. [23] Silica shells can also be used to protect UCNP surfaces from dissolution. In contrast to more complex polymeric coating, silica surfaces can be easily functionalized by a wide range of coupling agents and biomolecules, and the interior of the silica shell can be modified by integrating e. g. dye molecules. However, amorphous silica is a porous material, typical Stöber silica has a pore size around 1-4 nm, [36, 37] so that a thin silica coating cannot completely inhibit the dissolution of UCNP. [38] Though, the thickness of silica shells on UCNP can be easily adjusted over a wide range. [39] Lathinen et al. have shown that even a thin silica coating of < 2 nm or 5 nm can already reduce the luminescence quenching of UCNP in aqueous dispersion. [19] Besides, several

studies revealed that silica coated UCNP have a low toxicity compared with other nanoparticles *in vitro* and *in vivo*. [7, 11, 40]

In the present work, the cytotoxicity of UCNP cores coated with silica shells was investigated on the macrophage cell line RAW 264.7. RAW 264.7 cells are particularly sensitive to the treatment with nanoparticles [41] and have already been applied for studies with uncoated $NaGdF_4$ [41] and silica particles. [42, 43]

Upconversion cores consisting of $NaYF_4$ doped with 18% Yb and 2% Er were synthesized. Microporous silica shells with two different thicknesses were grown on them to investigate a possible relation between the degree of cytotoxicity and the particle size and silica shell thickness. The particles were subsequently functionalized with N-(6-aminohexyl)-aminopropyltrimethoxysilane (AHAPS) that provides a positive charge onto the nanoparticle surface to increase their interaction with the cell membrane. The particles were characterized by scanning transmission electron microscopy (STEM), dynamic light scattering (DLS), electrophoretic light scattering (ELS), and inductively coupled plasma optical emission spectrometry (ICP-OES). Before the cell experiments, their stability in the cell culture medium was investigated through DLS and ELS. The cytotoxicity of the UCNP was determined by MTT tests and the analysis of the cell cycle. The UCNP uptake potential was evaluated by flow cytometry through the measurement of light side scattering, which is proportional to changes in cell granularity or internal complexity.

Results and Discussion

Preparation and characterization of the upconversion nanoparticles

Oleate-functionalized NaYF$_4$: Yb, Er nanocrystals were prepared by a thermal decomposition method [44], yielding spherical particles with a low polydispersity (see Figure 1 A, STEM diameter (d_{STEM}) = of 33±2 nm). The hydrodynamic diameter (Z-average) was 47±1 nm (PDI = 0.38±0.05). ICP-OES measurements yielded a percentual molar ratio of Y: Yb: Er = [74±1] : [25±1] : [2±0.5]. The XRD diffractogram shows a predominantly hexagonal crystal structure (JCPDS No. 00-028-1192), which is typical for such UCNP (see Figure S1). [44] The core was coated with two different silica layers: 7±1 nm for the thin-shelled silica and 21±2 nm for thick-shelled silica (samples UC@thin and UC@thick, see Figure 1 B and C). The thicker silica shell should protect the UCNP core more efficiently than a thinner silica shell by reducing the diffusion of water molecules to the UCNP and also reducing possible leaking of ions from the core. The UC-emission spectrum shows the typical green and red Er^{3+} emission bands of Er- and Yb-doped NaYF$_4$ NP (see Figure S2) [45-47]. The shape of the UC luminescence spectra is not influenced by the thickness of the silica coating, as reported in our previous work [39]. Additionally, samples with the same two different shell thicknesses were surface-functionalized with N-(6-aminohexyl)-aminopropyltrimethoxysilane (AHAPS) (samples UC@thin_NH$_2$, and UC@thick_NH$_2$). AHAPS was chosen as a surface ligand, due to its ability to provide the particles with a positive surface charge. [48] Positively charged silica particles can more efficiently interact than negatively charged particles with the negatively charged cell membrane [42], which can also cause an enhanced uptake. [48, 49] This process was supported by the fact that the hydrodynamic diameter of the AHAPS-functionalized particles would be small enough for an endocytic uptake. [48] (3-Aminopropyl)trimethoxysilane

(APS) was not chosen as amine ligand due to the increased aggregation of APS functionalized particles in cell culture medium. [48]

In addition, particles were prepared where the coupling product of Rhodamine B isothiocyanate and APS (RBITC-APS) was coupled into the silica shell as an example for particles with a modified silica shell. Samples with two different thicknesses were prepared: 9 ± 2 nm for the thin-shelled samples and 22 ± 2 nm for the thick-shelled samples (samples UC@thin_RBITC_NH$_2$ and UC@thick_RBITC_NH$_2$). The silica shells of the dye-doped samples were slightly thicker than those of the samples without dye, as APS and RBITC-APS slightly increase the porosity of the silica shell. Consequently, identical amounts of silica per particle result in slightly thicker shell thicknesses. As a reference system, pure silica nanoparticles with a size of 50 nm were also coupled with RBITC and functionalized with AHAPS (sample SiO$_2$@RBITC_NH$_2$). STEM images for each sample are shown in Figure S3. The STEM data of all particles are summarized in Table 1.
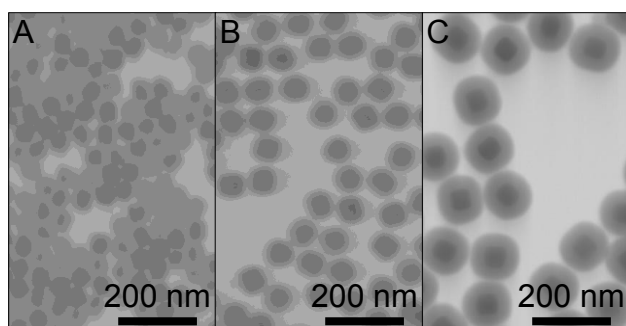
Figure 1: STEM image of (A) oleate-coated UCNP (NaYF$_4$: 18 % Yb, 2 % Er). (diameter = 33 ± 2 nm), (B) UC@thin (thickness of the silica shell (t_{SiO_2}) = 7 ± 2 nm); (C): UC@thick (t_{SiO_2} = 21 ± 3 nm).

Table 1: STEM diameter and silica shell as well as hydrodynamic diameter (z-average, Z-ave), polydispersity index (PDI), and zeta potential (ZP) of silica-coated UCNP in EtOH, water and supplemented DMEM complete medium.

Samples	d_{STEM} [nm]	t_{SiO_2} [nm]	EtOH			Water			DMEM	
			Z-ave [nm]	ZP [mV]	PDI	Z-ave [nm]	ZP [mV]	PDI	Z-ave [nm]	PDI
UC@thin_NH2	48±2	8±2	105±1	34±1	0.099±0.005	128±5	26±2	0.118±0.004	318±13	0.720±0.045
UC@thick_NH2	75±2	21±2	145±1	37±2	0.177±0.015	295±2	29±1	0.258±0.028	220±2	0.460±0.010
UC@thin_RBITC_NH2	50±2	9±2	127±1	30±2	0.117±0.014	138±2	26±1	0.172±0.028	97±8	0.575±0.098
UC@thick_RBITC_NH2	76±3	22±2	118±1	27±2	0.065±0.009	139±2	19±1	0.161±0.023	144±2	0.367±0.049
UC@thin	47±2	7±2	80±2	24±1	0.112±0.004	104±1	31±2	0.203±0.006	93 ±1	0.460±0.004
UC@thick	75±3	21±3	98±2	21±1	0.037±0.006	142±1	29±1	0.098±0.014	125±3	0.159±0.011
SiO2@RBITC_NH2	52±3	-	98±1	16±1	0.100±0.010	103±2	10±1	0.100±0.010	208±5	-

The dispersion behavior and changes of the surface charge of the samples in various media were studied by conducting DLS and ELS measurements in different media (ethanol, water, and Dulbecco's Modified Eagle Medium (DMEM) supplemented with 10 % fetal bovine serum (FBS), 1 % glutamine, 1 % fungizone and 1% penicillin). The DLS and ZP results are also shown in Table 1.

The zeta potential turned from negative to positive after AHAPS-functionalization, due to the positive surface charge of the amine group in the AHAPS -ligand. The zeta potentials of the AHAPS functionalized samples slightly decrease after a transfer from ethanol to water, as reported in several publications [48, 49], and consequently, their hydrodynamic diameters increase. The zeta potential of the non-functionalized particles is more negative in water than in ethanol, but also, in this case, the z-average increases.

The z-average of the samples after redispersion in DMEM were lower than in water, except for the samples UC@thin_NH2, UC@thick_RBITC_NH2, and

SiO$_2$@RBITC_NH$_2$. The lower z-average of these samples may indicate increased stabilization by a protein corona [49-53]. However, the high ionic strength of the cell culture medium (I = 168 mmol/L) reduces electrostatic stabilization. Besides, the proteins in the cell culture medium DMEM supplemented with 10% fetal bovine serum (FBS) contribute to the measured hydrodynamic diameters [48]. FBS consists mostly of bovine serum albumin. The z-average of the supplemented DMEM used in this study without particles was 13±1 nm, and the corresponding PDI = 0.380±0.003. This causes an additional reduction of the hydrodynamic diameter compared to water and also explained the broad PDI of the samples.

Izak-Nau et al. investigated the aggregation of silica nanoparticles that occurred after redispersion in buffer solution and physiological medium.[51] They reported that various proteins in medium containing FBS were adsorbed onto the surface of bare SiO$_2$ and amine-functionalized SiO$_2$ nanoparticles and formed a protein corona with a new surface charge, depending on the type of proteins that build the corona. The adsorbed protein corona consisting of the proteins present in FBS could increase or reduce the stability of the particles and, consequently, their hydrodynamic diameter. [50-53] The non-functionalized samples, which have a negative surface charge due to surface silanol groups, were more stable in the cell culture medium than the amino-functionalized particles, in line with previous findings [48, 51]. The adsorption of a protein corona makes the surface charge of nanoparticles more negative and hence reduces the stability of positively charged particles. [49, 54, 55] Although the particles in this work showed increased aggregation in DMEM, the particles can still be taken up in macrophages such as RAW 264.7 cells. [42] This is also indicated by different degrees of the cytotoxicity of the samples in RAW 264.7 cells, where the cytotoxicity of the samples was dose-dependent, and the flow cytometry results (see below).

Ion release experiments

For the investigation of released lanthanide ions, UC@thin_NH$_2$ and UC@thick_NH$_2$, as representative samples for thin and thick-shelled samples were redispersed in water.

For better comparison with the results of the cell culture studies (see below), samples with a concentration of 200 µg/mL silica-coated UCNP and 200 µg/mL calculated concentration of only the UCNP cores in the silica-coated samples were prepared, allowed to stand for 24 h, and centrifuged with centrifuge tubes with a filter unit (pore size: 3000 NWCO) to separate the UCNP from possibly released ions. A concentration of 200 µg/mL was chosen since this was the highest concentration used in the cytotoxicity experiments. Hence, the concentration of released ions would be representative for the maximum concentration of released ions, which should correlate to the cytotoxicity results. The filtrates were measured by ICP-OES regarding their content of Y^{3+}, Yb^{3+}, and Er^{3+}. Additionally, a certain amount of the three corresponding lanthanide chlorides was dissolved in water to reach lanthanide ion concentrations of 1±0.1 ppm and 2±0.1 ppm. These solutions were then centrifuged with the centrifuge tubes with a filter unit, and the filtrate was measured with ICP-OES to determine which percentual amount of the ions was filtered through the centrifuge filter.

Similar preliminary tests were also performed with the UCNP and lanthanide chlorides in DMEM. However, only Er^{3+} could be detected with a high measurement uncertainty in the filtrate of the solutions of the lanthanide chlorides. Lanthanide ions are known to bind with phosphate in phosphate-buffered saline (PBS) and form stable lanthanide phosphates. [20] As DMEM contains Na$_2$HPO$_4$, it can be assumed that the lanthanide ions will also bound to these mentioned compounds. Therefore, a quantitative analysis of the ion release was not performed in DMEM.

Table 2 shows the percentages of filtered ions detected by ICP-OES after 24 h of redispersion in water. Table S1 shows the amounts of detected filtered ions from an initial ion concentration of 1±0.1 ppm and 2±0.1 ppm after dissolution in water. The recovery rate of the ions in water was the lowest for Er^{3+} (around 6%) followed by Yb^{3+} (17-21%) and Y^{3+} (38-45%). Due to these results and the relatively low Er^{3+} content of the samples, the data for Er^{3+} were not further considered.

The sample UC@thin_NH$_2$ showed a significantly higher percentage of lanthanide ions released after 24 h of redispersion and centrifugation in water compared to UC@thick_NH$_2$ (see Table 2). However, the difference would have to be much larger if only the deceleration of the diffusion through the three times thicker shell would delay the dissolution of the UCNP.[56] The percentages for Y^{3+} release are generally significantly higher than for Yb. This can be partially explained by the lower content of Yb^{3+} and the lower and with falling concentration decreasing recovery rate of Yb^{3+} compared to Y^{3+}. Still, the difference is more significant than expected from these considerations. Lahtinen et al. have also observed that a significantly higher molar fraction of Y^{3+} than Yb^{3+} is released from NaYF$_4$: Yb, Er nanocrystals.[19] Dong et al. reported analogous observation for the ratio of Y^{3+} and Gd^{3+} at the partial disintegration of NaGdF$_4$:Y^{3+},Tb^{3+}.[57] This finding can be explained by assuming that Y^{3+} ions are concentrated on the nanoparticle surface and are consequently more dissolved compared to the other ions. [19]

The samples with 200 µg/mL silica-coated UCNP show a higher percentage of released ions compared to those with 200 µg/mL UCNP cores since the dissolution process of NaYF$_4$: Yb, Er UCNP in water is limited by its low solubility product. [58, 59] The ICP OES data show that the release of lanthanides from UCNP even with a silica coating is not negligible but that a thicker layer reduces this process. Lahtinen et al. reported that NaYF$_4$: Yb, Er particles with a similar diameter (26-31 nm) but just a

poly(acrylic acid) coating release more than 7% of their F^- in 24 h at a concentration 50 µg/mL. [19] This comparison suggests that already a 7 nm thick silica layer significantly reduces the disintegration process.

Table 2: Percentages of released lanthanide ions from silica-coated UCNP obtained by ICP-OES measurements after 24 h of dispersion in water.

Sample	c = 200 µg/mL UCNP cores		c = 200 µg/mL silica coated UCNP		
	Y [%]	Yb [%]	c (UCNP cores) [µg/mL]	Y [%]	Yb [%]
UC@thin_NH$_2$	0.97±0,01	0.18±0,03	96	1.88±0,07	0.41±0,05
UC@thick_NH$_2$	0.33±0,02	0.20±0,02	33	0.97±0,03	0.15±0,08

Cytotoxicity studies

Figure 2 shows the viability results for the RAW 264.7 cells upon exposure to UCNPs. The cytotoxicity of UC@thin_NH$_2$ in RAW 264.7 cells was higher than that of UC@thick_NH$_2$. At the highest particle concentration (c = 200 µg/mL), the cell viability after exposure to UC@thin_NH$_2$ was about 51±5 %, whereas, in the sample UC@thick_NH$_2$, the cell viability was 75±6 %. At the lowest concentration (c = 12.5 µg/mL) the cell viability was 110±12 % for UC@thin_NH$_2$ and 95±14 % for UC@thick_NH$_2$. UC@thin_RBITC_NH$_2$ caused a slightly higher cytotoxicity than UC@thin_NH$_2$, especially at lower concentrations of 12.5 and 25 µg/mL. At these concentrations, the cytotoxicity of the former sample was about 74±1 %. In general, UC@thick_NH$_2$ was the least cytotoxic particle type for all samples. At the highest

concentrations (c = 150 and 200 µg/mL) of UC@thick_NH$_2$, no significant difference in the cell viability was observed between the two concentrations. The cytotoxicity of pure silica without a UCNP core (sample SiO$_2$@RBITC_NH$_2$) was also measured. The cell viability at the lowest concentration was 83±5 %, and 68±4 % at the highest concentration, arguing for moderate cytotoxicity.
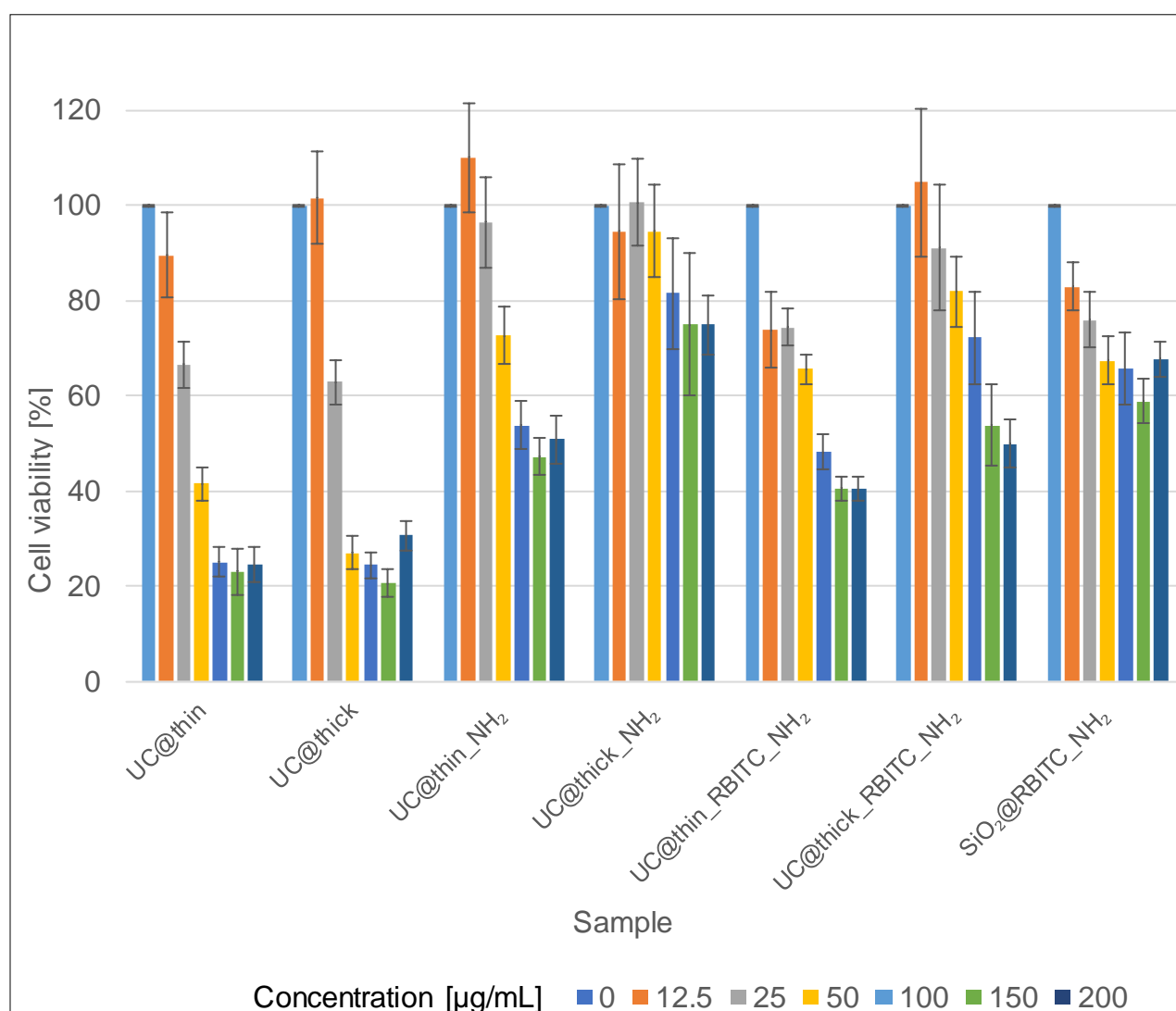
Figure 2: MTT assay results of silica-coated UCNP and SiO$_2$ nanoparticles on RAW 264.7 cells.

Both non-functionalized samples were more cytotoxic compared to the amino-functionalized particles. UC@thin exhibits an only slightly higher degree of cytotoxicity

than UC@thick. Nabeshi et al. investigated the cytotoxicity of non-modified, amine functionalized, and carboxyl functionalized 70 nm SiO_2 NP in RAW 264.7 cells. [43] They observed that unmodified SiO_2 nanoparticles had the highest cytotoxicity due to the higher degree of uptake into the cells. In contrast, the amine-functionalized particles were only adsorbed onto the cell membrane. Similar results were also obtained by Kurtz-Chalot et al., where highly positively charged SiO_2 nanoparticles were more adsorbed than taken up compared to the corresponding non-modified particles [42]. Xia et al. investigated cell type-dependent cytotoxicity for RAW 264.7, epithelial (BEAS-2B) cells, human microvascular endothelial (HMEC), hepatoma (HEPA-1), and pheochromocytoma (PC-12) cells after exposure to amine-functionalized polystyrene nanoparticles (NH_2-PS).[60] They observed that lysosomal permeabilization and mitochondrial damage happened in RAW 264.7 cells but not in other cell types. The particles were cytotoxic to RAW 264.7 and BEAS-2B cells but not to other cells. The nanoparticles perturbed the proton pump activity in RAW 264.7 cells, causing osmotic swelling and finally ruptured of the lysosomes.

According to these literature results, the RAW 264.7 cells internalize the negatively charged particles to a greater extent than the positively functionalized ones, causing the former particles to have higher cytotoxicity on RAW 264.7 cells, as it could also be observed in this work. Nevertheless, the thicker silica shell reduces the degree of cytotoxicity of the amino-functionalized samples in the macrophage cells more than that of non-functionalized particles. Possibly ions released at the cell membrane also can reduce cell viability.

The cell viability of the silica-coated particles in this work is dramatically higher than that of non-coated $NaGdF_4$ nanoparticles. Wysokińska et al. reported for such particles with average sizes between 4 and 249 nm IC50 values in MTS assays below 2 µg/mL. [41]

Cell uptake

Flow cytometry can provide qualitative and quantitative information about internalized particles in cells or those adsorbed onto cellular membranes, relying on the fact that cells that have internalized nanoparticles increase their internal complexity. [61, 62] Several publications have shown that the side scattering correlates with the concentration of nanoparticles attached or taken up by cells. [62-67]

The flow cytometry measurements were carried out with cells incubated with nanoparticles (c=100 µg/mL) for 24 h at 37 °C. Figure 3 shows SSC histograms of RAW 264.7 cells after exposure to UC@thin_NH$_2$ (blue framed area) and UC@thick_NH$_2$ (red framed area). The data for the non-particle-treated controls are marked as a yellow framed area. After 24 h, the SSC mean value for UC@thin_NH$_2$ was [251±8]·10^3, and that of UC@thick_NH$_2$ was [323 ±17]·10^3, while the control was [212±6]·10^3. The percentage increase of the SSC mean value for UC@thin_NH$_2$ was 18±5 % and 52±9 for UC@thick_NH$_2$, indicating a higher increase of cell granularity for UC@thick_NH$_2$; thus a higher uptake rate compared to the samples with the thin-shelled particles. The MTT cytotoxicity assay showed higher cytotoxicity for UC@thin_NH$_2$ compared to UC@thick_NH$_2$, which means the stronger increase side scattering signal of the thickly-coated particles does not correspond to higher cytotoxicity. So likely, although more thick-shelled particles were taken up, these are less toxic to the cells than a smaller quantity of thinner-shelled particles.

Figure 3 shows a bar chart of the SSC mean values for RAW 264.7 cells. The flow cytometry measurements of UC@thin and UC@thick were done at another time than the rest of the samples. Hence, they had their own negative (control) samples.

Mostly, the UCNP samples with thicker shells had higher SSC mean value than those with thin shells, indicating higher changes of cell granularity after exposure to the nanoparticles, i. e. a higher amount of incorporated particles. However, this does not

go along with higher cytotoxicity since the thinly-coated samples had a higher degree of cytotoxicity in the MTT test than the thickly-coated particles (see Figure 2). The cytotoxicity of the thinly-coated samples must have been caused by other effects that did not result in a stronger increase in cell granularity, such as the higher release of ions and a related reduction in cell viability, as it is indicated by ion release experiments and MTT data (see Figures 2 and 3).
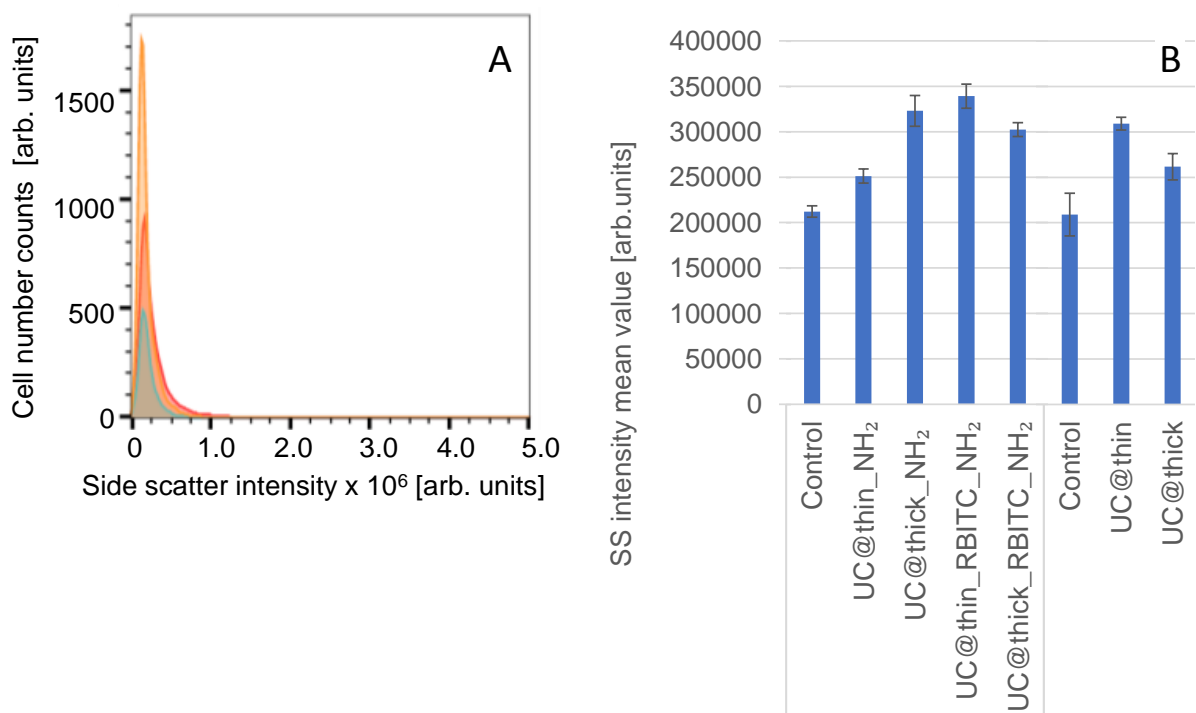
Figure 3: (A) SSC histograms of RAW 264.7 cells after particle exposure for 24 h at 37 °C. UC@thin_NH2 is marked by a blue framed peak; UC@thick_NH2 is marked by a red-framed peak, and the control is marked by a yellow framed peak. (B) Summary of mean SSC flow cytometry measurements on all samples in RAW 264.7 cells after 24 h at 37 °C.

Cell Cycle Analysis

To gain a deeper understanding of the effect of silica-coated UCNP on RAW 264.7 macrophages, an analysis of the cell cycle dynamics of the samples, UCNP@thin_NH$_2$ and UCNP@thick_NH$_2$ were exemplarily carried. The cell cycle consists of four parts: The rest phase (G0), the first gap phase (G1), where the cells grow and produce necessary enzymes for cell division, the synthesis phase (S), where the DNA is replicated, and the second gap phase (G2), where the cell continues to grows further and performs processes necessary for mitosis. [68] Both silica-coated samples show a significant increase in the G0/G1 phase compared to control cells not treated with nanoparticles (see Figure 4). Accordingly, the cell population in the S phase is reduced relative to the control. This effect is more pronounced for the sample with the thinner silica shell. In the case of sample UCNP@thin_NH$_2$, the percentage of the cell population in the second rest phase (G2) is strongly increased, whereas, for the sample UCNP@thick_NH$_2$, this percentage is comparable to that of the control. A calculation of the Proliferative Index (PI), according to Equation (1), shows that cells treated with both types of nanoparticles show a significantly decreased PI (0.39±0.05 for sample UCNP@thin_NH$_2$ and 0.35±0.14 for sample UCNP@thick_NH$_2$) compared to the control (0.53±0.06).

$$PI = \frac{S + G2/M}{G0/G1 + S + G2/M} \quad (1)$$

In contrast to this observation, the silica particles without a UCNP core (sample NP@SiO$_2$-RBITC-NH$_2$) exhibit a similar cell cycle dynamics as the nanoparticle-free control (see Figure S4 in the Supporting Information). Their PI is also similar

(0.54±0.10) to that of the control (0.48±0.06) and the control used for the other particles (0.53±0.06).

This observation of an affected cell cycle comprising longer rest phases and a shorter S phase, especially for the particles with a thinner silica shell, roughly correlates with the reduced cell viability of these samples in the MTT test. However, it is surprising that the cell cycle for the particles treated with UCNP-free silica particles is not significantly influenced. Similar findings suggesting a partial blocking of the cell cycle by UCNP were reported by Liu et al., who also observed a G0/G1 cell-cycle arrest and a significant decrease of the PI for colon endothelial cells (human adenocarcinoma (SGC-7901) cells) incubated with PVP-coated $NaYF_4$: Yb, Er particles in a similar concentration range.[68] Chen et al. investigated $NaYF_4$:Yb,Er nanoparticles capped with (aminomethyl)phosphonic (AMPA), (aminopropyl)triethoxysilane (APTES), and dihydrocinnamic acid (DHCA) on epithelial cells (Chinese Hamster ovary (CHO-K1) cells).[69] They observed that both, the positively charged AMPA and APTES UCNP, as well as the negatively charged DHCA capped particle leads to a severe dysregulation of the cell cycle. In contrast to the present results, the authors found a dramatic decrease in the proportion of cells in the G1 phase and a substantial increase in the proportion of cells in the G2 phase. The latter goes along with an increase in dead or lysed cells compared to the untreated control. In the study of Chen et al., the amino-functionalized UCNP were only surface-capped with the silane agent and no closed silica shell was grown around the particles, so that the release of cytotoxic ions was not reduced as in the present work.

Lu et al. investigated the effect of silica particles with various sizes and surface coatings on RAW.246.7 cells and found in agreement with our findings that amino-functionalized silica particles have only a negligible impact on the cell cycles if they are in the same size and concentration range as in the present work.[70] These results

suggest that a silica shell is a suitable coating material to reduce cytotoxicity. The effect of UCNP on RAW 246.7 cells has not been studied before.
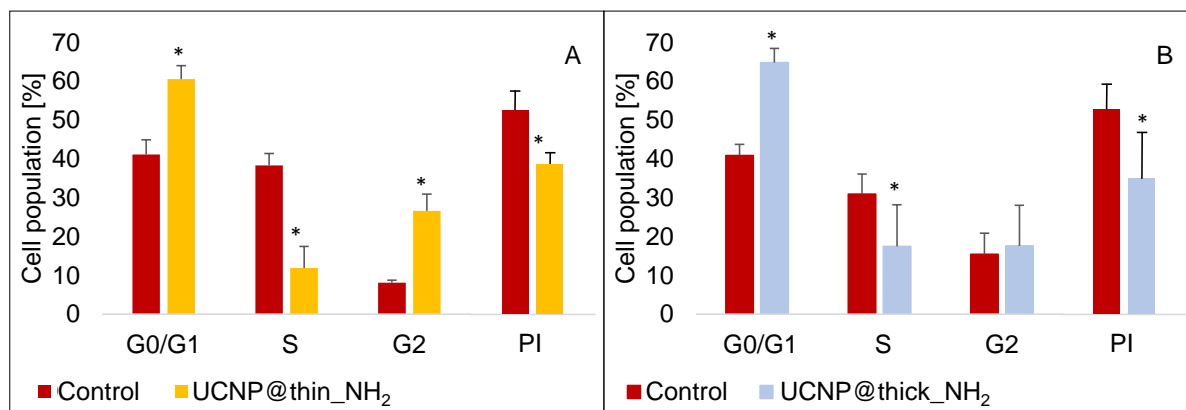
Figure 4: Effect of A: UC@thin_NH$_2$ (t_{SiO_2} = 8±2 nm) and B: UC@thick_NH$_2$ (t_{SiO_2} = 21±2 nm) on the cell cycle dynamics of RAW 264.7 macrophages after 24 h of exposure. The concentration was 200 µg/mL. * Indicates significant differences relative to the control p <0.05.

Conclusion

The presented data obtained on the effect of the coating of NaYF$_4$:Yb, Er nanocrystals with silica shells of two different thicknesses, indicate that coating UCNP with silica can be an efficient way to reduce the release of toxic ions from such particles and consequently their cytotoxicity. This assumption is well supported by cell viability, ion release, cell uptake and cell cycle analysis. Even if other factors, such as surface functionalization and subsequent effects such as agglomeration, also influence these processes. However, it also turned out that silica shells of 7 nm and even 21 nm thickness are not sufficient to completely hinder the release of lanthanide ions from UCNP, and as MTT tests and especially cell cycle analysis indicate, to reach for UCNP

a biocompatibility level similar to that of silica particles without a lanthanide core. It has to be considered that amorphous silica from a Stöber-like growth process is an inherently porous material with a pore size of 1-4 nm. [36, 37] Thus, it contains pores far larger than water molecules as well as lanthanide and other ions (Na^+ and F^-) contained in UCNP. An increase in the silica shell will likely further reduce the ions release. Moreover, ligands, which actively reduce the release/ dissolution process of lanthanide nanocrystals such as (multi)chelating phosphonates, [31, 33, 34] can be bound into or onto the surface of silica shells.[71] The use of different surfactants during the shell growth process might allow a slightly further reduction of the pore size. Silica coating of UCNP is a simple and well-established process. The thickness of the silica shell on UCNP can easily be adjusted over a wide range up to 200 nm [39]; hence it opens up not only a wealth of possibilities for (bio)-functionalization of UCNP [49] but also a simple approach to make UCNP less cytotoxic.

Experimental

All syntheses were performed with standard glass equipment. Before use, the reaction vessels were cleaned with hydrofluoric acid (8 vol. %) and subsequently repeatedly rinsed with water. The nanoparticles were redispersed using an ultrasonic bath (Sonorex RK512H (860 W, 35 kHz) from Bandelin). Ultrapure water (Millipore; filter size = 0.22 μm, R = 18.2 MΩ cm) was used for all syntheses.

Materials

Oleic acid (OA, 90 %), erbium chloride hexahydrate ($ErCl_3 \cdot 6H_2O$, 99.9 %), ytterbium chloride hexahydrate ($YbCl_3 \cdot 6H_2O$, 99.9 %), and yttrium chloride hexahydrate ($YCl_3 \cdot 6H_2O$, 99.9 %) were purchased from ABCR. N-(6-Aminohexyl)-aminopropyl

trimethoxysilane (AHAPS, 97%), 3-aminopropyltrimethoxysilane (APS, 99%), Rhodamine B-isothiocyanate (RBITC, ≥95%), polyoxyethylene (5) nonylphenylether (Igepal® CO-520), ammonium fluoride (NH_4F, 99.8 %), 1-octadecene (tech. 95 %), sodium oleate (82 %), tetraethyl orthosilicate (TEOS, 98 %), as well as erbium, yttrium, and ytterbium standards for ICP-OES measurements (TraceCERT®, c = 1000 mg/mL) were obtained from Sigma Aldrich. Cyclohexane (tech. 99.5 %) and ammonia water (p. a., 25 wt. % NH_3) were received from Roth. Ethanol (EtOH, 100 %) was purchased from Berkel AHK, hydrofluoric acid (HF, 30 %) from Riedel de Haën, and sodium hydroxide (NaOH, 99 %) from Grüssing.

Dulbecco's modified Eagle's medium (DMEM), fetal bovine serum (FBS), antibiotics, and phosphate buffer saline (PBS, pH 7.4) were purchased from Life Technologies (Carlsbad, CA, USA). 3-(4,5-dimethylthiazol-2-yl)-2,5-diphenyltetrazolium bromide (MTT), dimethyl sulfoxide (DMSO), propidium iodide (PI) and RNase were obtained from Sigma-Aldrich (St. Louis, MO, USA). The T-75 and T-25 flasks used to grow the cells, and the 12- and 96-well plates were from Corning®. Cell scrapers used to scrape off the RAW 264.7 cells attached to the surface of T-culture flasks were from PLC Labclinics.

All chemicals were used without further purification.

Synthesis

$NaYF_4$: Yb, Er UCNP were synthesized from the corresponding lanthanide oleates [72, 73] according to a modified procedure from Na et al. [44], which is described in detail in ref. [39].

Growth of the silica shell [39]

For a silica shell of 7±1 nm thickness, a dispersion of UCNP (diameter = 33±2 nm; c = 3 g/L) in 33.3 mL of cyclohexane was used. After sonication for 10 min, 3.736 mL of Igepal CO-520 was added, and after brief mixing using an ultrasonic bath, 0.331 mL of ammonia water were added, and the dispersion was again sonicated for 20 min. Subsequently, 0.331 mL of TEOS were added, and the whole mixture was sonicated for at least 1 h. Finally, the dispersion was stirred for 12 h at 1200 rpm at room temperature.

For the growth of a 21±2 nm thick silica shell first, additional cyclohexane, Igepal CO-520, and ammonia were added to the non-purified dispersion of UCNP coated with a 7±1 nm thick shell to maintain a surfactant concentration of 11 wt.% and a water concentration of a maximum of 2-3 wt.-%. The initial concentration of UCNP cores was set to 20 g/L, and the total volume was 5 mL. Next, 1.551 mL TEOS were added stepwise with a rate of 20.8 µL/min through a peristaltic pump (REGLO Digital MS–2/8–160 from Ismatec with a TYGON R-3603 tubing, type AME-01) while the dispersion was stirred for 12 h at 1200 rpm at room temperature. When the desired shell thickness was reached, the particles were precipitated by adding 5-10 mL of EtOH and purified three times by repeated centrifugation (1200 g, 1 h) and redispersion in 10 mL of EtOH and finally redispersed in 10-15 mL of EtOH.

For the growth of a silica shell with covalently bound RBITC, a modified method of Verhaegh et al. was used [74]. The reaction was carried under an inert atmosphere. The dye was first coupled with 3-aminopropyltrimethoxysilane yielding the dye coupling product RBITC-APS. For this, 2.7 mg ($5 \cdot 10^{-3}$ mmol) RBITC was diluted to 1 mM in dry EtOH and 10 µL ($5 \cdot 10^{-2}$ mmol) APS was added, and the solution was stirred overnight at room temperature in an inert atmosphere. The coupling product was not purified. The growth of the silica shell was performed as described above, besides that

ammonia was added as the last reagent and that after the addition of TEOS, 108 µL of the ethanolic solution of RBITC-APS were added dropwise continuously through a syringe in case of the particles with the thin silica shell for 100 mg mass of non-coated UCNP. 432 µL of this solution were added in the case of the second growth step of the thicker shell.

For providing a positive surface charge, the silica-coated UCNP were functionalized with AHAPS. The reaction was carried under inert atmosphere and is modified from earlier published work [75]. As an example, in case of the particles with the thin shell, 1.5 mL (c = 20 g/L in ethanol, particle mass = 30 mg) of the nanoparticle dispersion were diluted with ethanol to c = 1 g/L; a ten-time excess of 30 µL of AHAPS to ensure that the entire surface was covered by AHAPS and a few drops of ammonia water (30% v/v) to keep the pH at 9 were added. The mixture was stirred overnight in an argon atmosphere, followed by heating under reflux for 1 h. For the particles with the thicker silica coating, 1.5 mL (c = 20 g/L in ethanol; particle mass = 30 mg) of the dispersion were diluted to c = 1 g/L and reacted with 25 µL AHAPS and ammonia water. The nanoparticles were washed under inert atmosphere three times by repeated centrifugation (1200 g, 1 h) and redispersion in 10 mL of EtOH and finally redispersed in 10-15 mL of EtOH.

The silica particles without an UCNP core were prepared as described in ref. [48], besides that instead of fluorescein isothiocyanate rhodamine isothiocyanate was used. The functionalization with AHAPs was carried out by the same procedure, which was also used for the silica-coated UCNP.

Characterization

Scanning transmission electron microscopy (STEM)

STEM images were taken using a Hitachi SU 8030 scanning electron microscope with an electron acceleration voltage of 30 kV and a current of 20 µA. A droplet of a dispersion (c = 0.5-1 g/L) of the nanoparticles in either cyclohexane for oleate-functionalized UCNP cores or ethanol for silica-coated UCNP was dried on a carbon-coated copper grid (Cu 400 mesh, Quantifoil®: 100 carbon support films). The images were analyzed with the software FIJI.

Dynamic light scattering (DLS) and electrophoretic light scattering

The DLS and ELS measurements were performed with a Zetasizer Nano ZS from Malvern Instruments at 25 °C with a wavelength of 633 nm. The uncoated UCNP were dispersed in cyclohexane, and the silica-coated particles were dispersed in ethanol, water, or supplemented DMEM and filtered with a sterile syringe filter (pore size: 0.2 µm; materials: nylon for particles dispersed in cyclohexane and ethanol, and regenerated cellulose for particles dispersed in water or DMEM, Rotilab). Zeta potential measurements of the dispersions in ethanol and water were carried out with capillary zeta cells DTS 1070 from Malvern Instruments. In all measurements, the concentration of the samples was 0.5 - 1 mg/mL.

Ion release experiments

The silica-coated UCNP were redispersed in 4 mL ultrapure water or supplemented DMEM, so that final particle concentrations of 200 µg/mL of the silica-coated UCNP or the UCNP cores were obtained, left for 24 h at 37 °C, and centrifuged with centrifuge tubes with membrane filters (Amicon Ultracentrifuge, low binding Ultracelmembrane, 3000 Molecular Weight Cut-Off (MWCO)) for 2 h at 3080 g. Aliquots were then diluted

to 10 mL with ultrapure water and aqua regia (water: aqua regia = 4:1 v/v) and measured by ICP OES for determining the concentration of the Er^{3+}, Yb^{3+}, and Y^{3+} ions (see Supporting Information).

Aqueous solutions containing 1 and 2 ppm of Er^{3+}, Yb^{3+}, or Y^{3+} (prepared from the corresponding lanthanoid chlorides, see Section "Materials") were also centrifuged through the same Amicon filter tube mentioned above, diluted to 10 mL with ultrapure water and aqua regia (water : aqua regia = 4:1 v/v) and analyzed by ICP-OES for determining the concentration of Er^{3+}, Yb^{3+}, or Y^{3+} (see Supporting Information).

Cell culture of RAW 264.7 cells

RAW 264.7 cells were provided by the group of Dr. Philipp Seib at the University of Strathclyde, Glasgow, UK. The cells were grown in DMEM medium supplemented with 10 % fetal bovine serum (FBS), 2 mM L-glutamine, 100 U/mL penicillin, 100 µg/mL streptomycin, and 250 µg/mL fungizone at 37 °C in 5 % CO_2 humidified atmosphere [76]. The cells were daily observed for confluence and cell morphology using an inverted phase-contrast Eclipse TS100 microscope (Nikon, Tokyo, Japan). For routine subculturing, cells at ≈ 80 % confluency were gently lifted off by scrapping and transferred into fresh growth medium. For each experiment, cells were allowed to adhere for 24 h, and then the medium was replaced with fresh new medium containing UCNPs.

MTT cell viability assay

Cell viability was determined by the colorimetric changes of the MTT cytotoxicity assay. For that, 10^3 cells were seeded per well in a 96-well Corning® plate. Cells were then incubated for 24 h at 37 °C in 5 % CO_2 humidified atmosphere. After that, the culture medium was replaced with fresh medium containing UCNPs at 12.5; 25; 50; 100; 150;

200 µg/mL. RAW 264.7 cells exposed to culture medium were used as controls. Cells were exposed for 24 h, and after that, 50 µL of 3-(4,5-dimethylthiazole-2-yl)-2,5-diphenyltetrazolium bromide (MTT) at 1 mg /mL in PBS were added to each well, and the cells were incubated for another 4 h at 37 °C in 5 % CO_2. Afterward, 150 µL of DMSO was added to each well, and the plates were shaken in the dark using an orbital shaker (Mini Shaker Kisker Biotec). Absorbance was recorded at 570 nm using a microtiter plate reader (Synergy HT from BioTeK Instruments Inc).

The percentage of cell growth inhibition was calculated by the following Equation 2:

$$\% \text{ of inhibition} = \frac{\text{absorption at 570 nm from sample}}{\text{absorption at 570 nm from negative control}} \cdot 100\% \quad (2)$$

Cell Cycle Analysis

The cell cycle was analyzed by flow cytometry according to the method previously described.[77]. Briefly, cells were seeded in 6-well plates and incubated with UCNP at a concentration of 200 µg/mL. After exposure, cells were washed with PBS, harvested through scrapping, and centrifuged twice at 300g for 5 min. Cells were then fixed with 85% cold ethanol and kept at -20 ºC until analysis. At the time of analysis, cells were centrifuged at 300 g for 5 min, resuspended in PBS, and filtered through a 50-µm nylon mesh to separate aggregates. The cells were then incubated with 50 µL PI (1 mg/ml), a DNA intercalating fluorochrome, and 50 µL RNase (1 mg/ml) for 20 min, in the dark and at room temperature. Cell cycle distributions were assessed using a Beckman Coulter EPICS XL flow cytometer (Coulter Electronics, Hialeah, Florida, USA) and the percentage of cells in sub-G1, G0/G1, S, and G2 phases was determined by FlowJo software (FlowJo LLC, Ashland, OR, USA) applying the Watson Pragmatic model.

Uptake potential by flow cytometry

The uptake potential of UCNPs by RAW 264.7 cells by flow cytometry. RAW 264.7 cells were seeded (10^5 per well) in a 12-well plate and incubated for 24 h at 37 °C in 5 % CO2 humidified atmosphere for adherence. After that, the medium was replaced with fresh medium containing nanoparticles at concentration 100 μg/mL. Only fresh medium, without particles, was added to the controls/blank wells. Cells were incubated for 24 h at 37 ºC. After that, the supernatant was removed from each well, and cells were washed once with PBS. Then 1 mL supplemented DMEM was added, and finally, cells were collected by scraping and analyzed by flow cytometry in an Attune® Acoustic Focusing Cytometer (ThermoFisher Scientific). Both parameters, forward scatter (FS), which give information on the particle's size, and side scatter (SS), information on the complexity of particles, were measured.

Supporting Information

Supporting Information File 1:

File Name: Supporting Information_ Effect of Different Silica Coatings on the Toxicity of upconversion nanoparticles on RAW 264.7 macrophage cells_Kembuan et al.pdf

File Format: PDF

Title: Experimental details, additional UC luminescence spectra, XRD data, STEM images, ICP-OES, and cell cycle data.

Acknowledgments

References

1. Lu, Y. Q.; Zhao, J. B.; Zhang, R.; Liu, Y. J.; Liu, D. M.; Goldys, E. M.; Yang, X. S.; Xi, P.; Sunna, A.; Lu, J.; Shi, Y.; Leif, R. C.; Huo, Y. J.; Shen, J.; Piper, J. A.; Robinson, J. P.; Jin, D. Y. *Nat. Photon.* **2014**, *8* (1), 33-37.

2. Bettinelli, M.; Carlos, L. D.; Liu, X. *Phys. Today* **2015**, *68* (9).

3. Sun, S.-K.; Wang, H.-F.; Yan, X.-P. *Acc. Chem. Res.* **2018**, *51* (5), 1131-1143.

4. Li, Z.; Yuan, H.; Yuan, W.; Su, Q.; Li, F. *Coord. Chem. Rev.* **2018**, *354*, 155-168.

5. Li, X.; Zhang, F.; Zhao, D. *Chem. Soc. Rev.* **2015**, *44* (6), 1346-1378.

6. Jalani, G.; Tam, V.; Vetrone, F.; Cerruti, M. *J. Am. Chem. Soc.* **2018**, *140* (35), 10923-10931.

7. Zhou, M. Z.; Ge, X. Q.; Ke, D. M.; Tang, H.; Zhang, J. Z.; Calvaresi, M.; Gao, B.; Sun, L. N.; Su, Q. Q.; Wang, H. F. *Front. Chem.* **2019**, *7*.

8. Dukhno, O.; Przybilla, F.; Muhr, V.; Buchner, M.; Hirsch, T.; Mely, Y. *Nanoscale* **2018**, *10* (34), 15904-15910.

9. Oliveira, H.; Bednarkiewicz, A.; Falk, A.; Fröhlich, E.; Lisjak, D.; Prina-Mello, A.; Resch, S.; Schimpel, C.; Vrcek, I. V.; Wysokinska, E.; Gorris, H. H. *Adv. Healthc. Mater.* **2019**, *8* (1).

10. Plohl, O.; Kraft, M.; Kovac, J.; Belec, B.; Ponikvar-Svet, M.; Wurth, C.; Lisjak, D.; Resch-Genger, U. *Langmuir* **2017**, *33* (2), 553-560.

11. Kostiv, U.; Rajsiglova, L.; Luptakova, D.; Pluhacek, T.; Vannucci, L.; Havlicek, V.; Engstova, H.; Jirak, D.; Slouf, M.; Makovicky, P.; Sedlacek, R.; Horak, D. *RSC Adv.* **2017**, *7* (73), 45997-46006.

12. Zhou, L.; Wang, R.; Yao, C.; Li, X.; Wang, C.; Zhang, X.; Xu, C.; Zeng, A.; Zhao, D.; Zhang, F. *Nat. Commun.* **2015**, *6*.

13. Yang, D.; Ma, P. a.; Hou, Z.; Cheng, Z.; Li, C.; Lin, J. *Chem. Soc. Rev.* **2015**, *44* (6), 1416-1448.

14. Tsai, Y.-C.; Vijayaraghavan, P.; Chiang, W.-H.; Chen, H.-H.; Liu, T.-I.; Shen, M.-Y.; Omoto, A.; Kamimura, M.; Soga, K.; Chiu, H.-C. *Theranostics* **2018**, *8* (5), 1435-1448.

15. Su, Q.; Feng, W.; Yang, D.; Li, F. *Acc. Chem. Res.* **2017**, *50* (1), 32-40.

16. Chen, B.; Su, Q.; Kong, W.; Wang, Y.; Shi, P.; Wang, F. *J. Mater. Chem. B* **2018**, *6* (19), 2924-2944.

17. Green, K.; Huang, K.; Pan, H.; Han, G.; Lim, S. F. *Front. Chem.* **2018**, *6*.

18. Palo, E.; Salomaki, M.; Lastusaari, M. *J. Colloid Interf. Sci.* **2019**, *538*, 320-326.

19. Lahtinen, S.; Lyytikainen, A.; Pakkila, H.; Homppi, E.; Perala, N.; Lastusaari, M.; Soukka, T. *J. Phys. Chem. C* **2017**, *121* (1), 656-665.

20. Lisjak, D.; Plohl, O.; Vidmar, J.; Majaron, B.; Ponikvar-Svet, M. *Langmuir* **2016**, *32* (32), 8222-8229.

21. Dukhno, O.; Przybilla, F.; Muhr, V.; Buchner, M.; Hirsch, T.; Mély, Y. *Nanoscale* **2018**, *10* (34), 15904-15910, 10.1039/C8NR03892A.

22. Plohl, O.; Kralj, S.; Majaron, B.; Fröhlich, E.; Ponikvar-Svet, M.; Makovec, D.; Lisjak, D. *Dalton Trans.* **2017**, *46* (21), 6975-6984.

23. Estebanez, N.; Gonzalez-Bejar, M.; Perez-Prieto, J. *ACS Omega* **2019**, *4* (2), 3012-3019.

24. Lisjak, D.; Plohl, O.; Ponikvar-Svet, M.; Majaron, B. *RSC Adv.* **2015**, *5* (35), 27393-27397.

25. Mandl, G. A.; Cooper, D. R.; Hirsch, T.; Seuntjens, J.; Capobianco, J. A. *Methods Appl. Fluoresc.* **2019**, *7* (1), Review.

26. Agalakova, N. I.; Gusev, G. P. *ISRN Cell Biol.* **2012**, *2012*, 403835.

27. Barbier, O.; Arreola-Mendoza, L.; Maria Del Razo, L. *Chem.-Biol. Interact.* **2010**, *188* (2), 319-333.

28. Palasz, A.; Czekaj, P. *Acta Biochim. Pol.* **2000**, *47* (4), 1107-1114.

29. Gnach, A.; Lipinski, T.; Bednarkiewicz, A.; Rybka, J.; Capobianco, J. A. *Chem. Soc. Rev.* **2015**, *44* (6), 1561-1584.

30. Elsaesser, A.; Howard, C. V. *Adv. Drug Deliv. Rev.* **2012**, *64* (2), 129-137.

31. Li, R.; Ji, Z.; Dong, J.; Chang, C. H.; Wang, X.; Sun, B.; Wang, M.; Liao, Y.-P.; Zink, J. I.; Nel, A. E.; Xia, T. *ACS Nano* **2015**, *9* (3), 3293-3306.

32. Liu, J. N.; Bu, W. B.; Shi, J. L. *Acc. Chem. Res.* **2015**, *48* (7), 1797-1805.

33. Kostiv, U.; Lobaz, V.; Kučka, J.; Švec, P.; Sedláček, O.; Hrubý, M.; Janoušková, O.; Francová, P.; Kolářová, V.; Šefc, L.; Horák, D. *Nanoscale* **2017**, *9* (43), 16680-16688, 10.1039/C7NR05456D.

34. Li, R.; Ji, Z.; Chang, C. H.; Dunphy, D. R.; Cai, X.; Meng, H.; Zhang, H.; Sun, B.; Wang, X.; Dong, J.; Lin, S.; Wang, M.; Liao, Y.-P.; Brinker, C. J.; Nel, A.; Xia, T. *ACS Nano* **2014**, *8* (2), 1771-1783.

35. Hemmer, E.; Yamano, T.; Kishimoto, H.; Venkatachalam, N.; Hyodo, H.; Soga, K. *Acta Biomater.* **2013**, *9* (1), 4734-4743.

36. Li, S.; Wan, Q.; Qin, Z.; Fu, Y.; Gu, Y. *Langmuir* **2015**, *31* (2), 824-832.

37. Raschpichler, C.; Goroncy, C.; Langer, B.; Antonsson, E.; Wassermann, B.; Graf, C. M.; Klack, P.; Lischke, T.; Rühl, E. *J. Phys. Chem. C* **2020**.

38. Plohl, O.; Majaron, B.; Ponikvar-Svet, M.; Makovec, D.; Lisjak, D. *Acta Chimica Slovenica* **2015**, *62* (4), 789-795.

39. Kembuan, C.; Saleh, M.; Rühle, B.; Resch-Genger, U.; Graf, C. *Beilstein J. Nanotechnol.* **2019**, *10*, 2410-2421.

40. Wang, K.; Ma, J. B.; He, M.; Gao, G.; Xu, H.; Sang, J.; Wang, Y. X.; Zhao, B. Q.; Cui, D. X. *Theranostics* **2013**, *3* (4), 258-266.

41. Wysokinska, E.; Cichos, J.; Kowalczyk, A.; Karbowiak, M.; Strzadala, L.; Bednarkiewicz, A.; Kalas, W. *Biomolecules* **2019**, *9* (1).

42. Kurtz-Chalot, A.; Villiers, C.; Pourchez, J.; Boudard, D.; Martini, M.; Marche, P. N.; Cottier, M.; Forest, V. *ter. Sci. Eng. C-Mater. Biol. Appl.* **2017**, *75*, 16-24.

43. Nabeshi, H.; Yoshikawa, T.; Arimori, A.; Yoshida, T.; Tochigi, S.; Hirai, T.; Akase, T.; Nagano, K.; Abe, Y.; Kamada, H.; Tsunoda, S.; Itoh, N.; Yoshioka, Y.; Tsutsumi, Y. *Nanoscale Res. Lett.* **2011**, *6.*

44. Na, H.; Woo, K.; Lim, K.; Jang, H. S. *Nanoscale* **2013**, *5* (10), 4242-4251.

45. Chen, G. Y.; Qju, H. L.; Prasad, P. N.; Chen, X. Y. *Chem. Rev.* **2014**, *114* (10), 5161-5214.

46. Haase, M.; Schäfer, H. *Ang. Chem. Int. Ed.* **2011**, *50* (26), 5808-5829.

47. Fujii, M.; Nakano, T.; Imakita, K.; Hayashi, S. *J. Phys. Chem. C* **2013**, *117* (2), 1113-1120.

48. Graf, C.; Gao, Q.; Schütz, I.; Noufele, C. N.; Ruan, W.; Posselt, U.; Korotianskiy, E.; Nordmeyer, D.; Rancan, F.; Hadam, S.; Vogt, A.; Lademann, J.; Haucke, V.; Rühl, E. *Langmuir* **2012**, *28* (20), 7598-7613.

49. Zhang, J. P.; Liu, F. Y.; Li, T.; He, X. X.; Wang, Z. X. *RSC Adv.* **2015**, *5* (10), 7773-7780.

50. Wang, Y.; Zhao, Q. F.; Han, N.; Bai, L.; Li, J.; Liu, J.; Che, E. X.; Hu, L.; Zhang, Q.; Jiang, T. Y.; Wang, S. L. *Nanomed.-Nanotechnol. Biol. Med.* **2015**, *11* (2), 313-327.

51. Izak-Nau, E.; Voetz, M.; Eiden, S.; Duschl, A.; Puntes, V. F. *Part. Fibre Toxicol.* **2013**, *10*.

52. Monopoli, M. P.; Walczyk, D.; Campbell, A.; Elia, G.; Lynch, I.; Bombelli, F. B.; Dawson, K. A. *J. Am. Chem. Soc.* **2011**, *133* (8), 2525-2534.

53. Pisani, C.; Rascol, E.; Dorandeu, C.; Gaillard, J. C.; Charnay, C.; Guari, Y.; Chopineau, J.; Armengaud, J.; Devoisselle, J. M.; Prat, O. *Plos One* **2017**, *12* (8).

54. Qiu, Y.; Liu, Y.; Wang, L.; Xu, L.; Bai, R.; Ji, Y.; Wu, X.; Zhao, Y.; Li, Y.; Chen, C. *Biomaterials* **2010**, *31* (30), 7606-7619.

55. Lundqvist, M.; Stigler, J.; Elia, G.; Lynch, I.; Cedervall, T.; Dawson, K. A. *Proc. Nat. Acad.Sci.* **2008**, *105* (38), 14265-14270.

56. Lettinga, M. P.; van Zandvoort, M. A. M. J.; van Kats, C. M.; Philipse, A. P. *Langmuir* **2000**, *16* (15), 6156-6165.

57.   Dong, C.; Pichaandi, J.; Regier, T.; van Veggel, F. C. J. M. *J. Phys. Chem. C* **2011**, *115* (32), 15950-15958.

58.   Itoh, H.; Hachiya, H.; Tsuchiya, M.; Suzuki, Y.; Asano, Y. *Bull. Chem. Soc. Jpn.* **1984**, *57* (6), 1689-1690.

59.   Wu, D. X.; Wu, X. J.; Lv, Y. F.; Wang, H. *Mater. Lett.* **2008**, *62* (17-18), 3003-3006.

60.   Xia, T.; Kovochich, M.; Liong, M.; Zink, J. I.; Nel, A. E. *ACS Nano* **2008**, *2* (1), 85-96.

61.   Jochums, A.; Friehs, E.; Sambale, F.; Lavrentieva, A.; Bahnemann, D.; Scheper, T. *Toxics* **2017**, *5* (3).

62.   Suzuki, H.; Toyooka, T.; Ibuki, Y. *Environ. Sci. Technol.* **2007**, *41* (8), 3018-3024.

63.   Zucker, R. M.; Daniel, K. M.; Massaro, E. J.; Karafas, S. J.; Degn, L. L.; Boyes, W. K. *Cytom. Part A* **2013**, *83* (10), 962-972.

64.   Kumar, A.; Pandey, A. K.; Singh, S. S.; Shanker, R.; Dhawan, A. *Cytom. Part A* **2011**, *79A* (9), 707-712.

65.   Zucker, R. M.; Massaro, E. J.; Sanders, K. M.; Degn, L. L.; Boyes, W. K. *Cytom. Part A* **2010**, *77A* (7), 677-685.

66.   Toduka, Y.; Toyooka, T.; Ibuki, Y. *Environ. Sci. Technol.* **2012**, *46* (14), 7629-7636.

67.   Rosário, F.; Hoet, P.; Santos, C.; Oliveira, H. *Toxicology* **2016**, *368-369*, 103-115.

68.   Liu, C.; Chen, H.; Li, S. Y.; Xu, H.; Zhao, D. *J. Nanosci. Nanotechnol.* **2016**, *16* (4), 3653-3658.

69.   Chen, Y.; D'Amario, C.; Gee, A.; Duong, H. T. T.; Shimoni, O.; Valenzuela, S. M. *Acta Biomater.* **2020**, *102*, 384-393.

70.   Lu, X. Y.; Jin, T. T.; Zheng, J.; Fan, X. H. *J. Nanosci. Nanotechnol.* **2017**, *17* (2), 954-967.

71.   Duncan, A. K.; Klemm, P. J.; Raymond, K. N.; Landry, C. C. *J. Am. Chem. Soc.* **2012**, *134* (19), 8046-8049.

72.   Park, J.; An, K. J.; Hwang, Y. S.; Park, J. G.; Noh, H. J.; Kim, J. Y.; Park, J. H.; Hwang, N. M.; Hyeon, T. *Nat. Mater.* **2004**, *3* (12), 891-895.

73.   Wei, Y.; Lu, F. Q.; Zhang, X. R.; Chen, D. P. *Chem. Mater.* **2006**, *18* (24), 5733-5737.

74.   Verhaegh, N. A. M.; van Blaaderen, A. *Langmuir* **1994**, *10* (5), 1427-1438.

75.   Graf, C.; Gao, Q.; Schütz, I.; Noufele, C. N.; Ruan, W.; Posselt, U.; Korotianskiy, E.; Nordmeyer, D.; Rancan, F.; Hadam, S.; Vogt, A.; Lademann, J.; Haucke, V.; Rühl, E. *Langmuir* **2012**, *28*, 7598-7613.

76.   Bastos, V.; de Oliveira, J.; Brown, D.; Jonhston, H.; Malheiro, E.; Daniel-da-Silva, A. L.; Duarte, I. F.; Santos, C.; Oliveira, H. *Toxicol. Lett.* **2016**, *249*, 29-41.

77.   Oliveira, H.; Monteiro, C.; Pinho, F.; Pinho, S.; Ferreira de Oliveira, J. M. P.; Santos, C. *Mutat. Res. Genet. Toxicol. Environ. Mutagen.* **2014**, *775-776*, 38-47.